

1 **High-resolution regional climate modeling evaluation based on**
2 **varres-CESM and WRF over California**

3 Author One* and Author Two[†]

4 *American Meteorological Society, Boston, Massachusetts*

5 Extra Author

6 *Affiliation, City, State/Province, Country*

7 *Corresponding author address: Author One, American Meteorological Society, 45 Beacon St.,
8 Boston, MA 02108.

9 E-mail: latex@ametsoc.org

10 [†]Current affiliation: American Meteorological Society, 45 Beacon St., Boston, MA 02108.

ABSTRACT

11

¹² **1. Introduction**

¹³ Global climate models (GCMs) have been widely used to simulate both past and future climate.

¹⁴ Although GCMs have been demonstrated to successfully represent large-scale features of the cli-

¹⁵ mate system, they have usually been employed at coarse resolutions (~ 1 degree), largely due to

¹⁶ computation limitations. The climate reanalysis datasets, which assimilate climate observations

¹⁷ within climate model, can represent a best estimate of historical weather patterns, but still have

¹⁸ low resolution no finer than 0.5 degree. Under this circumstance, regional climate is not well

¹⁹ captured by global climate models (GCMs) and global reanalysis datasets which are employed at

²⁰ coarse resolutions. And dynamic processes at unrepresented scales are significantly drivers for

²¹ regional and local climate variability especially over complex terrain (Soares et al. 2012). In or-

²² der to capture those fine-scale dynamical features, high horizontal resolution is needed to allow a

²³ more accurate representation of fine scale forcing, and the better representation of processes and

²⁴ interactions, as former studies have already showed (Leung et al. 2003; Rauscher et al. 2010).

²⁵ Also, better represented regional climate information can lead to effective action for responses to

²⁶ climate change and mitigation of negative impacts taken by local stakeholders and policymakers.

²⁷ In order to model regional climate at a higher spatial and temporal resolution over a limited area,

²⁸ downscaling methods have been developed. There are two main downscaling ways. One is sta-

²⁹ tistical methodology, it aims to estimate finer scale properties through analyzing the relationships

³⁰ between observed variables at different scales (Fowler et al. 2007). This method is empirical and

³¹ cannot be used if the observed relationships do not hold with a changing climate (Soares et al.

³² 2012). The other is called dynamical downscaling, using numerical model to simulate higher spa-

³³ tial resolution conditions in greater detail. The dynamical downscaling method is most popular and

³⁴ commonly used. Two type of models are used including nested limited-area models (LAMs) and

variable-resolution (including stretched-grid) global climate models (VRGCMs) (Laprise et al. 2008). The more commonly used LAMs are often referred as regional climate models (RCMs) when applying to climate scales. RCMs are forced by output of GCMs or reanalysis data, and have been widely used, showing the ability to capture physically consistent regional and local circulations at the needed spatial and time scales (Christensen et al. 2007; Bukovsky and Karoly 2009; Caldwell et al. 2009; Mearns et al. 2012). For the VRGCM approach, it uses a variable-resolution global model composing high-resolution over a specific region and lower resolution over the rest of the globe (Staniforth and Mitchell 1978; Fox-Rabinovitz et al. 1997). VRGCMs have been shown to be an alternative way for regional climate studies and applications, owing the advantages of traditional GCMs in representing large-scale features, and also being computationally less expensive than uniform GCMs (Fox-Rabinovitz et al. 2001, 2006).

Compared with RCMs, a key advantage of VRGCMs is the use a single model rather than the combinations of GCM and RCM. Thus, VRGCMs avoid potential lack of consistency between the driver and model, and naturally allow two-way interaction between the high-resolution area and the global domain without nudging (Warner et al. 1997; McDonald 2003; Laprise et al. 2008; Mesinger and Veljovic 2013). In order to get deeper insight for the performances of these two different modeling methods, it is necessary to compare them directly. The goal of this paper is to evaluate the performance of VRGCMs together with the traditional method of RCMs for the first time to see whether VRGCMs can show similar or even better ability in regional climate modeling. And simulations will be conducted at higher resolution than most former studies. This will add value in modeling mean regional climatology and improve our understanding about the effects of multi-scale processes in regional climate regulation. In this study, WRF (Weather Research and Forecasting) is used as a traditional RCM method (Skamarock et al. 2005). WRF has gained wide acceptance to study regional climate over the past decade, showing its adequate capability

59 in representation of mean fine-scale climate properties (Lo et al. 2008; Leung and Qian 2009;
60 Soares et al. 2012). For the VRGCM approach, the newly developed variable-resolution CESM
61 (varres-CESM) is adopted here. CESM is a state-of-the-art Earth modeling framework developed
62 at NCAR, consisting of atmospheric, oceanic, land and sea ice components (Neale et al. 2010).
63 However, variable-resolution in Community Atmosphere Models (CAM) Spectral Element (SE)
64 dynamical core is a recently available technique which has never be applied for long-term regional
65 climate simulation (Taylor and Fournier 2010; Zarzycki et al. 2014).

66 Simulations using both methods have been implemented for 26 years historical climate centered
67 on the state of California (CA). With the complex topography, coastal influence, and wide latitude
68 range, it makes CA a suitable test bed for high-resolution climate studies. Also, it is necessary to
69 learn detailed local climate variability in California with its important agricultural role and socioe-
70 conomic status, and particular vulnerability to anthropogenically-induced climate change (Hayhoe
71 et al. 2004; Cayan et al. 2008). RCM simulations over California have been conducted in previ-
72 ous studies (Leung et al. 2004; Kanamitsu and Kanamaru 2007; Caldwell et al. 2009; Pan et al.
73 2011; Pierce et al. 2013). Caldwell et al. (2009) presented results from WRF (Weather Research
74 and Forecasting) at 12km spatial resolution showing both the overall consistent and certain bias
75 between the simulations and observations (Caldwell et al. 2009). The paper is organized as fol-
76 lows. Section 2 describes the model set up, evaluation methods and verification data. In Section 3,
77 results are demonstrated focusing on 2 m temperature (Ts) and precipitation (Pr). Key results are
78 summarized and further discussion is made in section 4.

79 **2. Models and Methodology**

80 *a. Simulation design*

81 1) WRF

82 The fully compressible non-hydrostatic WRF-ARW model in version 3.5.1 is used. ERA-
83 Interim pressure-level reanalysis was used to provide initial, lateral conditions and SST for the
84 domains every 6 h. ERA-Interim reanalysis (~ 80 km) has been widely used and shows its strong
85 reliability as forcing data (Dee et al. 2011). Two simulations are conducted for 27km (WRF27)
86 and 9km (WRF9) horizontal resolution separately from 1979-01-01 to 2005-12-31 (UTC). The 10
87 km resolutions are actually finer than most former studies for long-term climate.

88 For the coarser resolution, one domain is used. For the WRF9, two nested domains are settled
89 with outer domain at 27km (same as the WRF27) and inner domain at 9km horizontal grid spacing,
90 with two-way nesting. Both grids are centered at CA and have respectively, 120*110 and 151*172
91 grid points. 10 grid points are used as lateral relaxation zones. Sea surface temperature (SST) was
92 updated due to the long-term climate modeling. In order to reduce the drift between forcing data
93 and RCM over time, grid nudging (Stauffer and Seaman 1990) was applied to the outer domain
94 per 6 hours at all levels except the planetary boundary layer (PBL) as suggested by Lo et al. (Lo
95 et al. 2008). This setup uses 41 vertical levels with top pressure at 50hpa.

96 We use the following parameterization options for the standard settings: WSM 6-class graupel
97 microphysics scheme (Hong and Lim 2006), Kain-Fritsch cumulus scheme (Kain 2004), CAM
98 shortwave and longwave radiation schemes (Collins et al. 2004) (??). These settings are supported
99 by the one-year test running result with different options. Also, the Yonsei University (YSU)
100 boundary layer scheme (Hong et al. 2006), and Noah Land Surface Model (Chen and Dudhia
101 2001) are chosen as commonly used (?? add citations here) for climate applications considering

¹⁰² long-term reliability and computational cost. Figure 1 shows the study region and topography for
¹⁰³ each domain.

¹⁰⁴ 2) VARRES-CESM

¹⁰⁵ CESM has been under development for nearly two decades, and has been used heavily in bet-
¹⁰⁶ ter understanding the effects of global climate change (Hurrell et al. 2013). Here, CAM version
¹⁰⁷ 5 (CAM5) and Community Land Model (CLM) version 4 are used. As we have mentioned, re-
¹⁰⁸ cently, SE as the default dynamical core in CAM has added variable resolution support. Here, the
¹⁰⁹ variable-resolution cubed-sphere grids are generated within both CAM and CLM with the open-
¹¹⁰ source software package SQuadGen (citation??). Simulations at 0.25 degree ($\sim 28\text{km}$) and 0.125
¹¹¹ degree ($\sim 14\text{km}$) horizontal resolution are developed, remaining regrid is at 1 degree, also with
¹¹² time period from 1979-01-01 to 2005-12-31 (UTC). Corresponding fine-scale topography is pro-
¹¹³ duced. Land surface data at 50 km resolution is used. Tuning parameters and other necessary
¹¹⁴ setting options are tested to reach our need. Greenhouse gas (GHG) concentrations are prescribed
¹¹⁵ based on observations. SSTs and ice coverage are supplied by the 1degree Hadley Centre Sea Ice
¹¹⁶ and Sea Surface Temperature dataset (HadISST) (Hurrell et al. 2008).

¹¹⁷ Figure 2 shows the grid mesh for each simulation.

¹¹⁸ *b. Methodology*

¹¹⁹ The evaluation focuses on near surface air temperature and precipitation to display the mean
¹²⁰ regional climate variability both annually and seasonally. Reanalysis and gridded observational
¹²¹ datasets (described in Table 1) are employed as reference data compared against simulation results
¹²² to assess the models' performances. Due to the uncertainties in observations, we use different
¹²³ sources of datasets including measurements from stations, high-resolution reanalysis data or satel-

¹²⁴ lite information. Though these products are generally based on similar measurements, they are
¹²⁵ scaled and gridded using different techniques, causing processing uncertainty except of measure-
¹²⁶ ment error. And we acknowledge that reanalysis products can not be treated as truth.

¹²⁷ The UW daily gridded meteorological data is obtained from the Surface Water Modeling group
¹²⁸ at the University of Washington (Maurer et al. 2002). The PRISM monthly gridded climate obser-
¹²⁹ vations is produced by the PRISM (Parameter elevation Regression on Independent Slopes Model)
¹³⁰ Climate Group, and the dataset is based on a larger network of station data and accounts for el-
¹³¹ evation and topographic effects (cite??). UW Ts dataset is computed similarly to Pr, but without
¹³² the topographic adjustment towards PRISM, and using a simple 6.1 K/km lapse rate. The Daymet
¹³³ gridded daily meteorological observations also take into account areas of complex terrain. The Na-
¹³⁴ tional Oceanic and Atmospheric Administration (NOAA) Climate Prediction Center (CPC) dataset
¹³⁵ uses more stations than the UW data, but without topographic correction (cite??). The National
¹³⁶ Centers for Environmental Prediction (NCEP) North American Regional Reanalysis (NARR) is
¹³⁷ NCEP's high resolution combined model and assimilated dataset (cite??).

¹³⁸ In order to keeping consistency, reference data are interpolated to models' output resolution
¹³⁹ when showing the differences or calculating related statistical values (e.g. root mean square er-
¹⁴⁰ rror (RMSE), bias, and correlation). Bilinear interpolation method is used for regular 2D grid.
¹⁴¹ Also, output from globally uniform CESM with 25km spatial resolution is compared together to
¹⁴² see if variable-resolution CESM perform similarly or even better in modeling mean climatology
¹⁴³ (Bacmeister et al. 2014). The first year was treated as model spin-up, thus, all the data analysis are
¹⁴⁴ based on the period from 1980 to 2005, i.e. 26 years.

¹⁴⁵ In order to get in-depth analysis of California's varied climate regions, here we divide the state
¹⁴⁶ into 5 regional zones as Figure 1 shows.

¹⁴⁷ **3. Results**

¹⁴⁸ Topographic details within different models and diverse horizontal scales are showed in Figure
¹⁴⁹ 3. We can see that higher resolutions own better representation of topography, which is important
¹⁵⁰ driver for fine-scale dynamic processes especially at complex terrain. In this part, we will show
¹⁵¹ the models' performances in both temperature and precipitation. In this section, comparisons and
¹⁵² analysis are focused on daily maximum, minimum and average 2m temperatures (Tmax, Tmin and
¹⁵³ Tavg), and daily precipitation (Pr) both annually and seasonally. These variables are most relevant
¹⁵⁴ for climate assessment.

¹⁵⁵ *a. Temperature*

¹⁵⁶ The long-term annual average climatology of Tmax, Tmin and Tavg from varres-CESM, uni-
¹⁵⁷ form CESM, WRF and reference dataset are displayed by Fig. 4, 5 and 6. Generally, simu-
¹⁵⁸ lations show similar regional patterns as observations, with warmer central valley and southern
¹⁵⁹ deserts, and colder northern coastal area and Sierra mountainous region. Both WRF and variable-
¹⁶⁰ resolution CESM demonstrate satisfactory modeling ability. And higher resolution simulations
¹⁶¹ perform better capturing fine features close to observations, especially for WRF 9km. Comparing
¹⁶² with uniform CESM, varres-CESM performed similarly or even better in some cases, showing
¹⁶³ both improved modeling ability at high resolution and reduced computation cost.

¹⁶⁴ However, they do display some differences in different sub zones. In particular, Tmax are a little
¹⁶⁵ higher mainly at central valley in both CESM and WRF, and WRF 9km shows much more obvious
¹⁶⁶ cold bias in other regions than other simulations. Varres-CESM perform better than WRF and
¹⁶⁷ uniform CESM, especially at higher resolution. However, Tmin is obviously warmer by both WRF
¹⁶⁸ and CESM, especially at coastal region and southern desert, resulting under-prediction of diurnal
¹⁶⁹ range. WRF and uniform CESM perform better than varres-CESM. The differences between

models and reference data are plotted in Fig. 7 for Tavg, in order to show the output comparison more clearly. Varres-CESM and WRF perform similarly, better than uniform CESM. Comparing with PRISM, models show overall underestimation, especially at coastal and mountain regions, however with relatively small bias at most region. The RMSE for these models are basically ranges from 1 to 3 K, as showed by Table 2. Overall, variable-resolution CESM 0.125 deg performs best for long-term annual results, however, WRF 9km has larger error than WRF 27km. (varres-CESM \downarrow WRF \downarrow uniform CESM). And Correlations are high between simulations and observations (>0.95), especially for Tmax and Tavg. There are about +2 K SST bias near the coast between varres-CESM and WRF. This may explain part of the reason for the above results. NARR shows obvious differences from other gridded observations, however, uncertainty between observational datasets are much smaller than the models' biases, unlikely impacting our results.

The seasonal cycle of Tavg is showed in Figure 8. Models do show good consistent with reference data with about no larger than 2 K bias, mainly in coldest and hottest seasons. However, varres-CESM do show smaller bias than WRF at summer season except over mountain region, and WRF did better at winter season. Varres-CESM seems to be colder in winter and WRF is not hot enough in summer. And varres-CESM showed larger variability among seasons than observations, while WRF shows opposite trend. No obvious divergence can be detected between multi-scales, though coarser simulations even result a littler better than finer ones. Also, seasonal trends are similar among sub-zones, though showing diverse magnitudes, and models seem to perform less better over coastal region. As for the multi-year monthly variability, models are quite close to reference dataset around 4 K, except in winter season, especially at January, varres-CESM and WRF 9km show about half time and one time larger values respectively.

For CA, we are more interested in the summer season, especially the Tmax value for heat extreme analysis. Here, the annually average summer Tmax from models and reference data are

194 displayed in Figure 9 and 10. CESM generally overestimate Tmax especially for uniform CESM
195 except at coastal region, while WRF showed obviously negative bias expect at central valley.
196 Varres-CESM with higher resolution performed best as proved by the statistics in Table 3, how-
197 ever, WRF 27km show less error than WRF 9km. Overall, models especially varres-CESM 0.125d
198 and WRF 9km still show fairly accuracy over most regions. The underlying reasons behind those
199 differences can be manifold including the models' inner mechanism, the forcing data and the
200 scale effects. In order to further investigate the models' ability for heat extreme detection, we
201 also depicted the frequency distribution of Tmax constructed from 26 years summer daily data in
202 Figure 11. Normal distributions are showed by both models and observations, though biases are
203 noticed between them (even within observations). Models are more consistent with observations
204 over upper bound than lower bound. For hot events detection, both varres-CESM and WRF 27km
205 exhibit satisfactory performance over most regions. No obvious improvement is showed by higher
206 resolution in varres-CESM.

207 *b. Precipitation*

208 The long-term annual average climatology of daily precipitation (Pr) from varres-CESM, WRF
209 and reference dataset are displayed by Fig. 12 and 13. Comparing with observations, simula-
210 tions do capture regional patterns of precipitation. Precipitation distributes mostly along the north
211 coastal part and Sierra mountains, and relatively low over other regions. However, there exist
212 obvious differences among simulations. Varres-CESM overestimate a little especially for coarser
213 simulation at the western side of Sierras, and finer simulation has reduced that bias showing the
214 improvementnt of orographic effects. Comparing with varres-CESM, uniform CESM shows little
215 difference overall, though with obviously less bias over central valley. Notably, large difference
216 showed between WRF 27km and WRF 9km. WRF 27km underestimated a little, but WRF 9

greatly showed obvious positive absolute error at North coastal part and the Sierra where maximum precipitation is distributed, and the relative bias can reach 50 percent. Overall, models perform satisfactorily except for WRF 9km, and varres-CESM 0.125d perform a little better than CESM 0.25d and WRF 27km, as further showed by the RMSE and bias value in Table 4. Observations also demonstrate noticeable differences indicating uncertainty inherent in interpolating station data to a grid. However, these observations are still of the highest quality available and the uncertainty is relatively small comparing the simulations, and our conclusions can hold.

The climatological annual cycle of precipitation averaged over each sub regions is presented in Fig. 14. It can be seen that bias mainly occurred during rainy seasons especially in winter. WRF 27km is more consistent with observations than others. Varres-CESM is wetter especially in winter season. WRF 9km is too wetter. And WRF 27km is drier. As temperature, varres-CESM showed larger variability among seasons than observations, while WRF 27km shows opposite trend. The seasonal trend proves what we know about the strong seasonality of California Pr with high values during the winter and almost no precipitation during the summer.

In this way, we particularly showed the annually average winter precipitation from models and reference data as plotted in Figure 15 and 16. We can see that models and reference data show similar pattern as annual, though the precipitations almost doubles in winter comparing with annual value. Varres-CESM still overestimate with larger absolute bias, especially at central valley, and higher resolution still performs better. Uniform CESM overestimate over part of northern coast and mountain regions. WRF 27km underestimate a little, and WRF 9km still greatly overestimate at North coastal region and the sierra region. Considering the relatively heavy winter precipitation, the relative error is still acceptable for Varres-CESM, uniform CESM and WRF 27km, with RMSE and bias values showed in Table 5. Further, the frequency distribution of winter Pr constructed from 26 years daily data is depicted in Figure 17. It can be seen that varres-CESM is

more consistent with observations except at Central Valley, where WRF 27km performs much better as former figures already showed. Varres-CESM 0.25d and varres-CESM 0.125d do not show meaningful differences. However, WRF 27km shows underprediction of rainy days, especially for moderately rainy events, and, not surprisingly, WRF 9km obviously over-prediction rainy days particular when raining goes stronger. For strong precipitation events, varres-CESM and WRF 27 shows satisfactory modeling ability over most regions except at Central Valley for varres-CESM, though observations also show uncertainties.

The positive bias of precipitation using WRF at high resolution has also been found in former studies (Caldwell et al. 2009). Caldwell et al. (2009) gave a detailed discuss of the possible reasons, stating that bias comes from a variety of source like the model itself and partly the physics schemes. And this is out of the scope of this paper, further discussion can be found in former studies (Jankov et al. 2005; Gallus Jr and Bresch 2006).

At last, a concise summary of model performance annually over CA is provided by the Taylor diagram (Figure 18). This diagram includes the spatial correlation between the simulated and observed fields, the RMS variability of simulations normalized by that in the observations, and mean biases from verification data symbolized at (1,0).

4. Discussions and summary

scale effect, extreme analysis, precipitation parameterization

Acknowledgments.

References

Bacmeister, J. T., M. F. Wehner, R. B. Neale, A. Gettelman, C. Hannay, P. H. Lauritzen, J. M. Caron, and J. E. Truesdale, 2014: Exploratory high-resolution climate simulations using the

- 263 community atmosphere model (cam). *Journal of Climate*, **27** (9), 3073–3099.
- 264 Bukovsky, M. S., and D. J. Karoly, 2009: Precipitation simulations using wrf as a nested regional
265 climate model. *Journal of Applied Meteorology and Climatology*, **48** (10), 2152–2159.
- 266 Caldwell, P., H.-N. S. Chin, D. C. Bader, and G. Bala, 2009: Evaluation of a wrf dynamical
267 downscaling simulation over california. *Climatic Change*, **95** (3-4), 499–521.
- 268 Cayan, D. R., A. L. Luers, G. Franco, M. Hanemann, B. Croes, and E. Vine, 2008: Overview of
269 the california climate change scenarios project. *Climatic Change*, **87** (1), 1–6.
- 270 Chen, F., and J. Dudhia, 2001: Coupling an advanced land surface-hydrology model with the
271 penn state-ncar mm5 modeling system. part i: Model implementation and sensitivity. *Monthly
272 Weather Review*, **129** (4), 569–585.
- 273 Christensen, J. H., and Coauthors, 2007: Regional climate projections. *Climate Change, 2007:*
274 *The Physical Science Basis. Contribution of Working group I to the Fourth Assessment Report
275 of the Intergovernmental Panel on Climate Change, University Press, Cambridge, Chapter 11,*
276 847–940.
- 277 Collins, W. D., and Coauthors, 2004: Description of the ncarr community atmosphere model (cam
278 3.0). Tech. rep., Tech. Rep. NCAR/TN-464+ STR.
- 279 Dee, D., and Coauthors, 2011: The era-interim reanalysis: Configuration and performance of the
280 data assimilation system. *Quarterly Journal of the Royal Meteorological Society*, **137** (656),
281 553–597.
- 282 Fox-Rabinovitz, M., J. Côté, B. Dugas, M. Déqué, and J. L. McGregor, 2006: Variable resolution
283 general circulation models: Stretched-grid model intercomparison project (sgmip). *Journal of
284 Geophysical Research: Atmospheres (1984–2012)*, **111** (D16).

- 285 Fox-Rabinovitz, M. S., G. L. Stenchikov, M. J. Suarez, and L. L. Takacs, 1997: A finite-difference
286 gcm dynamical core with a variable-resolution stretched grid. *Monthly weather review*, **125** (11),
287 2943–2968.
- 288 Fox-Rabinovitz, M. S., L. L. Takacs, R. C. Govindaraju, and M. J. Suarez, 2001: A variable-
289 resolution stretched-grid general circulation model: Regional climate simulation. *Monthly*
290 *weather review*, **129** (3), 453–469.
- 291 Gallus Jr, W. A., and J. F. Bresch, 2006: Comparison of impacts of wrf dynamic core, physics
292 package, and initial conditions on warm season rainfall forecasts. *Monthly weather review*,
293 **134** (9), 2632–2641.
- 294 Hayhoe, K., and Coauthors, 2004: Emissions pathways, climate change, and impacts on california.
295 *Proceedings of the National Academy of Sciences of the United States of America*, **101** (34),
296 12 422–12 427.
- 297 Hong, S.-Y., and J.-O. J. Lim, 2006: The wrf single-moment 6-class microphysics scheme (wsm6).
298 *Asia-Pacific Journal of Atmospheric Sciences*, **42** (2), 129–151.
- 299 Hong, S.-Y., Y. Noh, and J. Dudhia, 2006: A new vertical diffusion package with an explicit
300 treatment of entrainment processes. *Monthly Weather Review*, **134** (9), 2318–2341.
- 301 Hurrell, J. W., J. J. Hack, D. Shea, J. M. Caron, and J. Rosinski, 2008: A new sea surface temper-
302 ature and sea ice boundary dataset for the community atmosphere model. *Journal of Climate*,
303 **21** (19), 5145–5153.
- 304 Hurrell, J. W., and Coauthors, 2013: The community earth system model: A framework for col-
305 laborative research. *Bulletin of the American Meteorological Society*, **94** (9), 1339–1360.

- 306 Jankov, I., W. A. Gallus Jr, M. Segal, B. Shaw, and S. E. Koch, 2005: The impact of different wrf
307 model physical parameterizations and their interactions on warm season mcs rainfall. *Weather*
308 and forecasting, **20 (6)**, 1048–1060.
- 309 Kain, J. S., 2004: The kain-fritsch convective parameterization: an update. *Journal of Applied*
310 *Meteorology*, **43 (1)**, 170–181.
- 311 Kanamitsu, M., and H. Kanamaru, 2007: Fifty-seven-year california reanalysis downscaling at 10
312 km (card10). part i: System detail and validation with observations. *Journal of Climate*, **20 (22)**,
313 5553–5571.
- 314 Laprise, R., and Coauthors, 2008: Challenging some tenets of regional climate modelling. *Meteo-*
315 *rology and Atmospheric Physics*, **100 (1-4)**, 3–22.
- 316 Leung, L. R., L. O. Mearns, F. Giorgi, and R. L. Wilby, 2003: Regional climate research: needs
317 and opportunities. *Bulletin of the American Meteorological Society*, **84 (1)**, 89–95.
- 318 Leung, L. R., and Y. Qian, 2009: Atmospheric rivers induced heavy precipitation and flooding
319 in the western us simulated by the wrf regional climate model. *Geophysical research letters*,
320 **36 (3)**.
- 321 Leung, L. R., Y. Qian, X. Bian, W. M. Washington, J. Han, and J. O. Roads, 2004: Mid-century
322 ensemble regional climate change scenarios for the western united states. *Climatic Change*,
323 **62 (1-3)**, 75–113.
- 324 Lo, J. C.-F., Z.-L. Yang, and R. A. Pielke, 2008: Assessment of three dynamical climate down-
325 scaling methods using the weather research and forecasting (wrf) model. *Journal of Geophysical*
326 *Research: Atmospheres (1984–2012)*, **113 (D9)**.

- 327 Maurer, E., A. Wood, J. Adam, D. Lettenmaier, and B. Nijssen, 2002: A long-term hydrologically
328 based dataset of land surface fluxes and states for the conterminous united states*. *Journal of*
329 *climate*, **15 (22)**, 3237–3251.
- 330 McDonald, A., 2003: Transparent boundary conditions for the shallow-water equations: testing in
331 a nested environment. *Monthly weather review*, **131 (4)**, 698–705.
- 332 Mearns, L. O., and Coauthors, 2012: The north american regional climate change assessment
333 program: overview of phase i results. *Bulletin of the American Meteorological Society*, **93 (9)**,
334 1337–1362.
- 335 Mesinger, F., and K. Veljovic, 2013: Limited area nwp and regional climate modeling: a test of the
336 relaxation vs eta lateral boundary conditions. *Meteorology and Atmospheric Physics*, **119 (1-2)**,
337 1–16.
- 338 Neale, R. B., and Coauthors, 2010: Description of the ncar community atmosphere model (cam
339 5.0). *NCAR Tech. Note NCAR/TN-486+ STR*.
- 340 Pan, L.-L., S.-H. Chen, D. Cayan, M.-Y. Lin, Q. Hart, M.-H. Zhang, Y. Liu, and J. Wang, 2011:
341 Influences of climate change on california and nevada regions revealed by a high-resolution
342 dynamical downscaling study. *Climate dynamics*, **37 (9-10)**, 2005–2020.
- 343 Pierce, D. W., and Coauthors, 2013: Probabilistic estimates of future changes in california temper-
344 ature and precipitation using statistical and dynamical downscaling. *Climate Dynamics*, **40 (3-4)**, 839–856.
- 345 Rauscher, S. A., E. Coppola, C. Piani, and F. Giorgi, 2010: Resolution effects on regional climate
346 model simulations of seasonal precipitation over europe. *Climate dynamics*, **35 (4)**, 685–711.

- 348 Skamarock, W., J. Klemp, J. Dudhia, D. Gill, and D. Barker, 2005: Coauthors, 2008: A description
349 of the advanced research wrf version 3. ncar technical note. Tech. rep., NCAR/TN-475+ STR.
- 350 Soares, P. M., R. M. Cardoso, P. M. Miranda, J. de Medeiros, M. Belo-Pereira, and F. Espírito-
351 Santo, 2012: Wrf high resolution dynamical downscaling of era-interim for portugal. *Climate*
352 *dynamics*, **39 (9-10)**, 2497–2522.
- 353 Staniforth, A. N., and H. L. Mitchell, 1978: A variable-resolution finite-element technique for
354 regional forecasting with the primitive equations. *Monthly Weather Review*, **106 (4)**, 439–447.
- 355 Stauffer, D. R., and N. L. Seaman, 1990: Use of four-dimensional data assimilation in a limited-
356 area mesoscale model. part i: Experiments with synoptic-scale data. *Monthly Weather Review*,
357 **118 (6)**, 1250–1277.
- 358 Taylor, M. A., and A. Fournier, 2010: A compatible and conservative spectral element method on
359 unstructured grids. *Journal of Computational Physics*, **229 (17)**, 5879–5895.
- 360 Warner, T. T., R. A. Peterson, and R. E. Treadon, 1997: A tutorial on lateral boundary conditions
361 as a basic and potentially serious limitation to regional numerical weather prediction. *Bulletin*
362 *of the American Meteorological Society*, **78 (11)**, 2599–2617.
- 363 Zarzycki, C. M., C. Jablonowski, and M. A. Taylor, 2014: Using variable-resolution meshes to
364 model tropical cyclones in the community atmosphere model. *Monthly Weather Review*, **142 (3)**,
365 1221–1239.

366 **LIST OF TABLES**

367	Table 1. Reanalysis or statistically downscaled observational datasets	20
368	Table 2. RMSE for annual Temperature	21
369	Table 3. Bias for annual Temperature	22
370	Table 4. RMSE and Bias for summer Tmax	23
371	Table 5. RMSE and Bias for annual Pr	24
372	Table 6. RMSE and Bias for DJF Pr	25

TABLE 1. Reanalysis or statistically downscaled observational datasets

Data source	Variables used	Spatial resolution	Temporal resolution
UW	Pr, T_{min} , T_{max}	0.125°	daily
PRISM	Pr, T_{min} , T_{max} , T_{avg}	4km	monthly/daily
DAYMET	Pr, T_{min} , T_{max}	1km	daily
NCEP CPC	Pr	0.125°	daily
NARR	Pr, T_s	32km	daily

TABLE 2. RMSE for annual Temperature

RMSE	UW		PRISM			DAYMET	
	T _{max}	T _{min}	T _{max}	T _{min}	T _{avg}	T _{max}	T _{min}
Varres CESM 0.25d	1.605	3.035	2.098	2.393	1.753	2.109	3.170
Varres CESM 0.125d	1.226	2.804	1.772	2.227	1.501	1.871	2.884
uniform CESM 0.25d	2.566	2.558	2.949	2.437	2.418	2.958	2.826
WRF 27km	1.710	2.506	2.240	1.729	1.721	2.105	2.691
WRF 9km	2.517	2.769	2.732	1.764	1.420	2.581	2.752

TABLE 3. Bias for annual Temperature

BIAS	UW		PRISM			DAYMET	
	T _{max}	T _{min}	T _{max}	T _{min}	T _{avg}	T _{max}	T _{min}
Varres CESM 0.25d	-0.082	2.385	-0.353	1.296	-0.269	-0.037	2.256
Varres CESM 0.125d	-0.241	2.229	-0.559	1.130	-0.438	-0.224	2.031
uniform CESM 0.25d	-0.409	1.402	-0.672	0.312	-0.907	-0.361	1.272
WRF 27km	-0.379	1.409	-0.649	0.321	-0.729	-0.336	1.282
WRF 9km	-1.805	2.166	-2.123	1.067	-0.891	-1.786	1.967

TABLE 4. RMSE and Bias for summer Tmax

Tmax	UW		PRISM		DAYMET	
	RMSE	Bias	RMSE	Bias	RMSE	Bias
Varres CESM 0.25d	2.324	0.982	2.932	0.631	2.810	1.177
Varres CESM 0.125d	1.903	0.651	2.452	0.233	2.477	0.824
uniform CESM 0.25d	3.872	1.788	4.265	1.449	4.300	1.988
WRF 27km	2.311	-0.574	2.924	-0.925	2.511	-0.383
WRF 9km	3.319	-2.274	3.470	-2.693	3.203	-2.101

TABLE 5. RMSE and Bias for annual Pr

Pr	CPC		UW		PRISM		DAYMET	
	RMSE	Bias	RMSE	Bias	RMSE	Bias	RMSE	Bias
Varres CESM 0.25d	0.590	0.370	0.604	0.265	0.726	0.171	0.560	0.169
Varres CESM 0.125d	0.481	0.220	0.534	0.126	0.634	0.050	0.510	0.043
uniform CESM 0.25d	0.551	0.118	0.601	0.012	0.708	-0.082	0.603	-0.083
WRF 27km	0.424	-0.210	0.586	-0.315	0.777	-0.409	0.650	-0.411
WRF 9km	2.204	1.462	2.026	1.368	1.858	1.292	1.986	1.286

TABLE 6. RMSE and Bias for DJF Pr

Pr	CPC		UW		PRISM		DAYMET	
	RMSE	Bias	RMSE	Bias	RMSE	Bias	RMSE	Bias
Varres CESM 0.25d	1.409	0.883	1.401	0.558	1.636	0.465	1.310	0.404
Varres CESM 0.125d	1.236	0.666	1.273	0.362	1.436	0.307	1.210	0.234
uniform CESM 0.25d	1.353	0.273	1.440	-0.052	1.566	-0.146	1.419	-0.206
WRF 27km	0.918	-0.396	1.331	-0.721	1.588	-0.815	1.389	-0.876
WRF 9km	4.244	2.562	3.801	2.257	3.538	2.203	3.782	2.132

373 LIST OF FIGURES

374	Fig. 1. Domains of WRF simulations (left: 9km, right: 27km) and topography (unit: m)	27
375	Fig. 2. The grid mesh of varres-CESM (left:0.25 degree, right:0.125 degree)	28
376	Fig. 3. Topography representations of simulations and ERA-Interim (unit: m)	29
377	Fig. 4. Annual average daily maximum 2m temperatures (Tmax) from models and reference datasets (unit: C)	30
379	Fig. 5. Similar as Fig. 4, but for daily minimum 2m temperatures (Tmin)	31
380	Fig. 6. Similar as Fig.4, but for daily mean 2m temperatures (Tavg)	32
381	Fig. 7. Difference between simulations and reference data for daily Tavg	33
382	Fig. 8. Seasonal cycle of monthly-average Tavg for each subzone (unit: C) Errorbars represent ? values	34
384	Fig. 9. Similar as Fig.4, but for summer Tmax	35
385	Fig. 10. Similar as Fig. 7 but for summer Tmax (the number is RMSE value)	36
386	Fig. 11. Frequency distribution of summer Tmax constructed from 26 years daily data (unit: C)	37
387	Fig. 12. Annual average daily precipitation (Pr) from models and reference datasets (unit: mm/d)	38
388	Fig. 13. Difference between simulations and reference data for Pr	39
389	Fig. 14. Simiarl as Figure 8, but for monthly-average Pr	40
390	Fig. 15. Similar as Figure 12, but for winter Pr	41
391	Fig. 16. Similar as Figure 13, but for winter Pr	42
392	Fig. 17. Frequency distribution of winter Pr constructed from 26 years daily data (unit: mm/d) (note: vertical scale is logarithmic)	43
394	Fig. 18. Taylor diagram of annual climatology for the region of CA, using PRISM dataset as reference	44

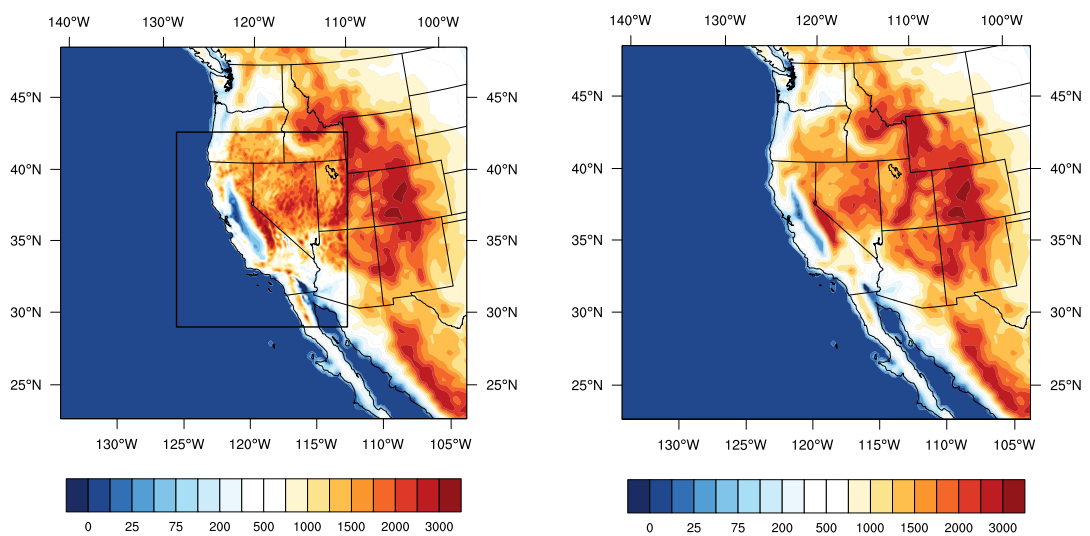


FIG. 1. Domains of WRF simulations (left: 9km, right: 27km) and topography (unit: m)

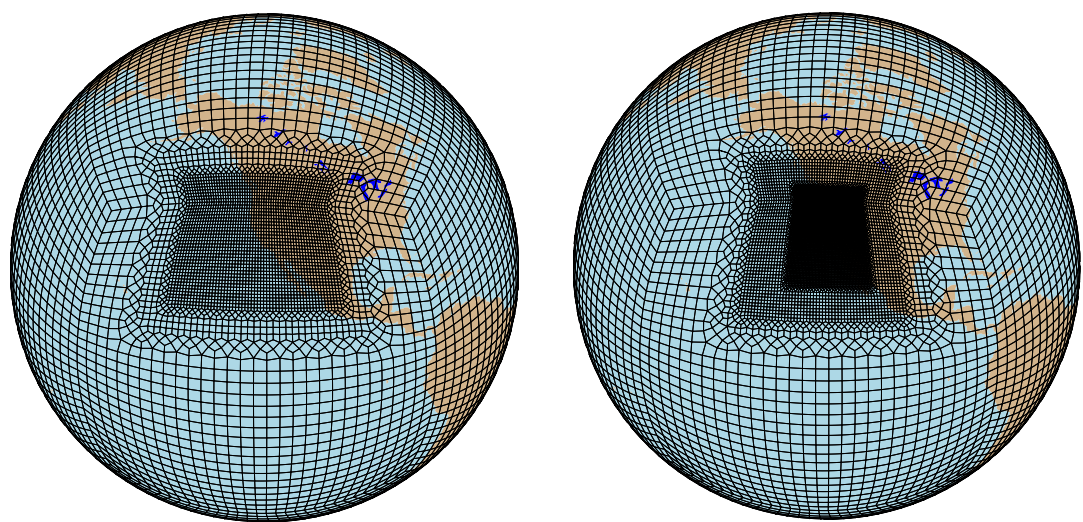


FIG. 2. The grid mesh of varres-CESM (left:0.25 degree, right:0.125 degree)

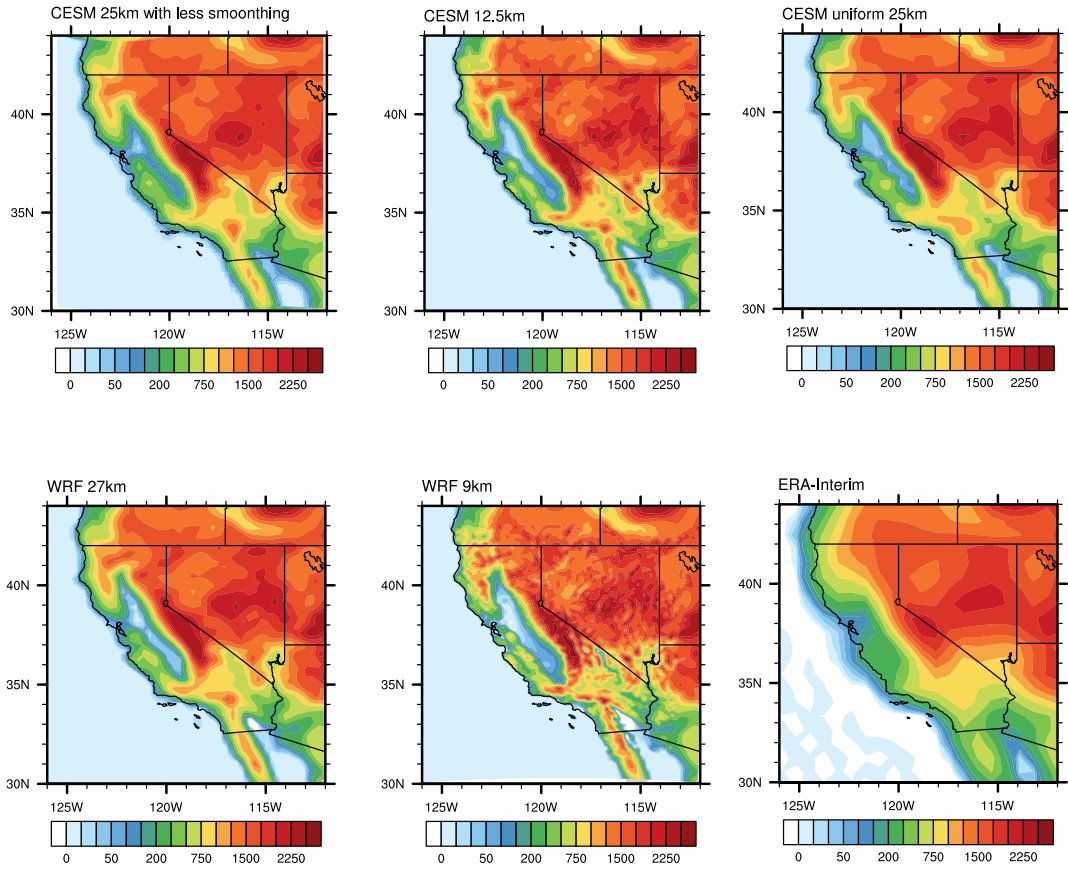


FIG. 3. Topography representations of simulations and ERA-Interim (unit: m)

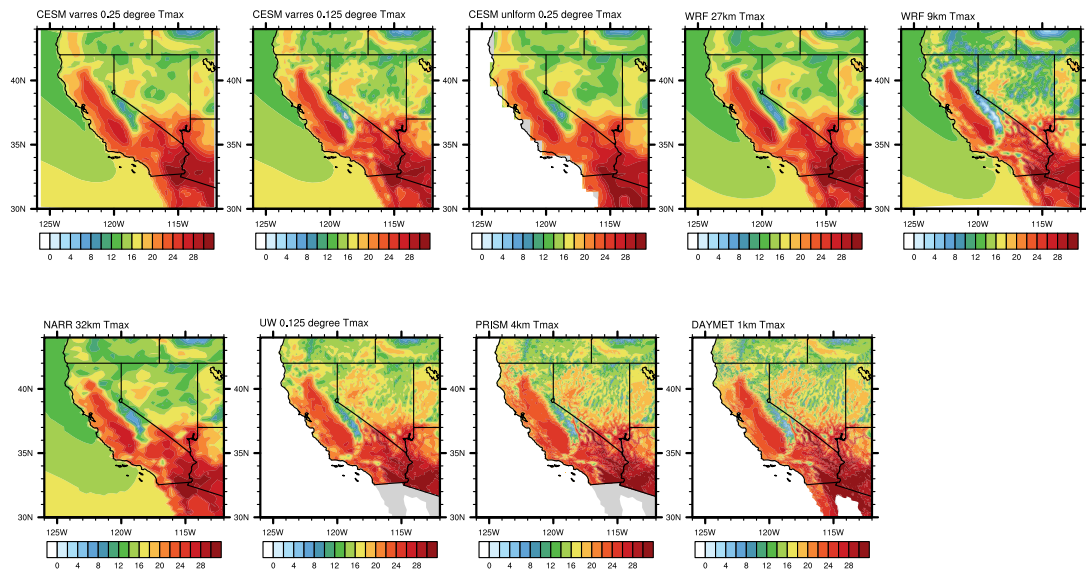


FIG. 4. Annual average daily maximum 2m temperatures (Tmax) from models and reference datasets (unit: C)

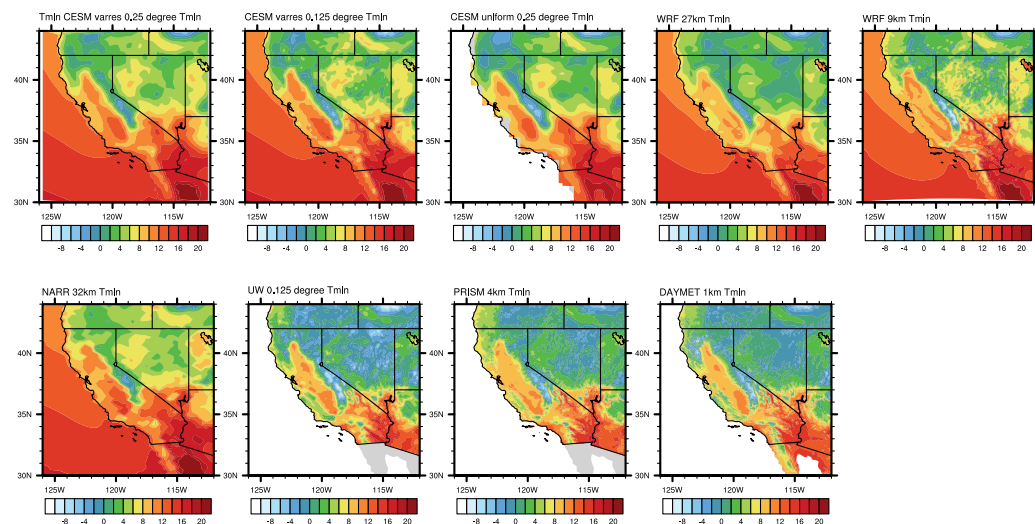


FIG. 5. Similar as Fig. 4, but for daily minimum 2m temperatures (Tmin)

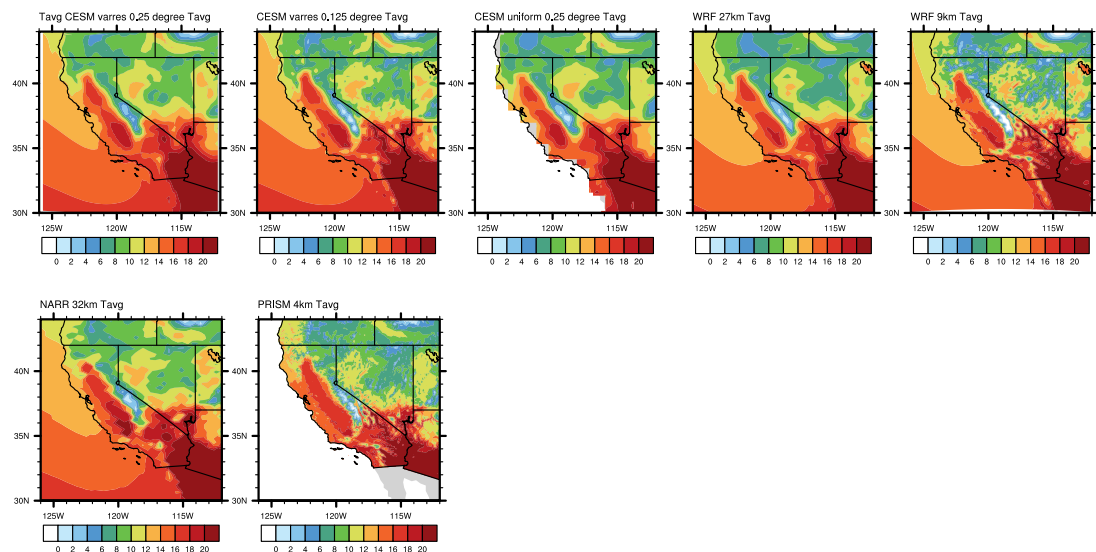


FIG. 6. Similar as Fig.4, but for daily mean 2m temperatures (Tavg)

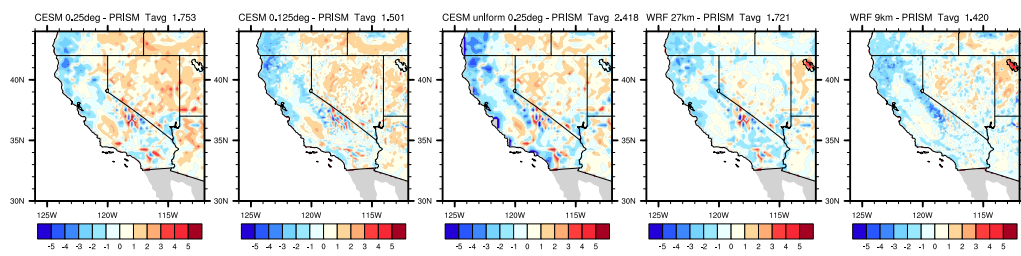


FIG. 7. Difference between simulations and reference data for daily Tavg

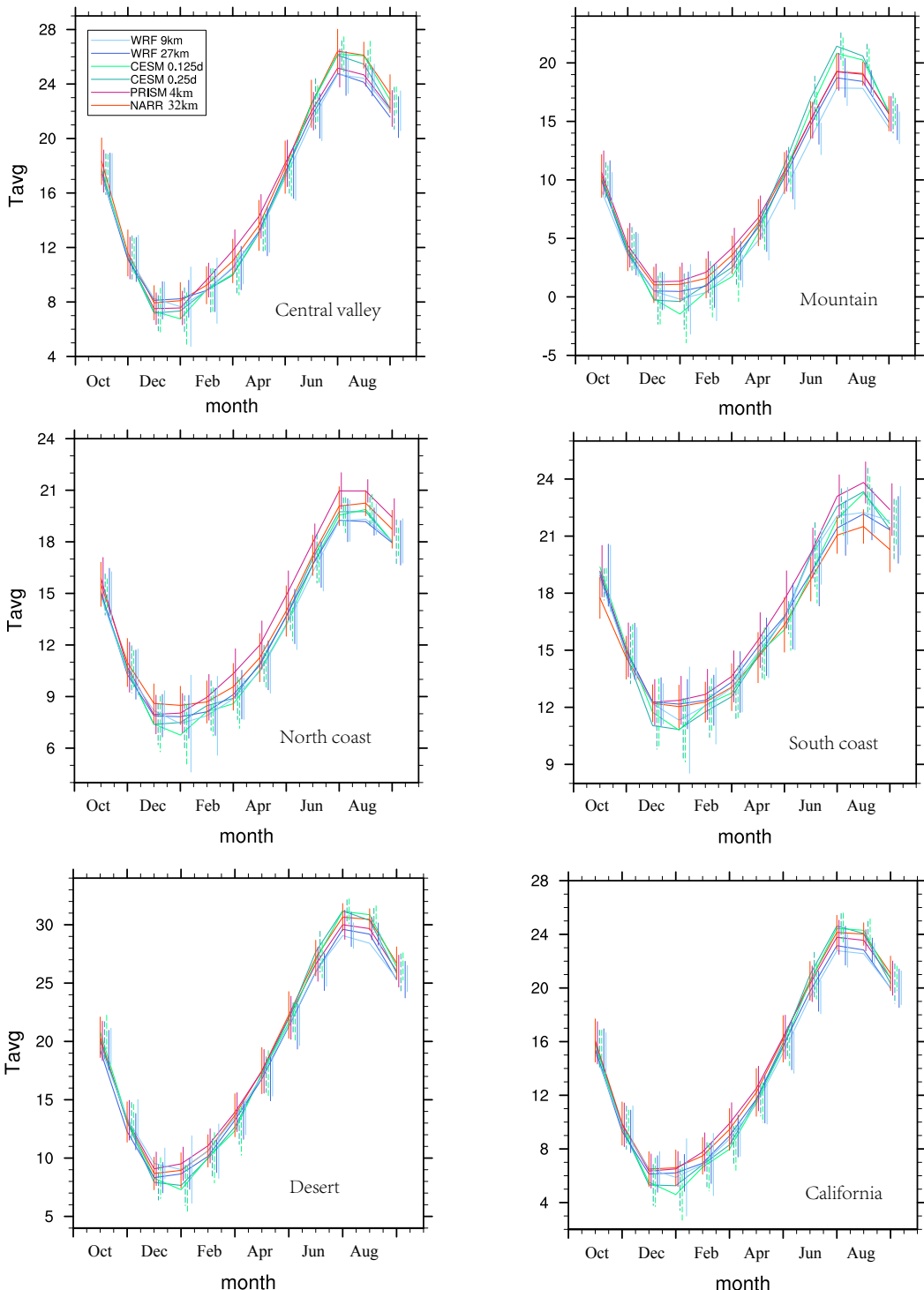


FIG. 8. Seasonal cycle of monthly-average Tavg for each subzone (unit: $^{\circ}\text{C}$) Errorbars represent ? values

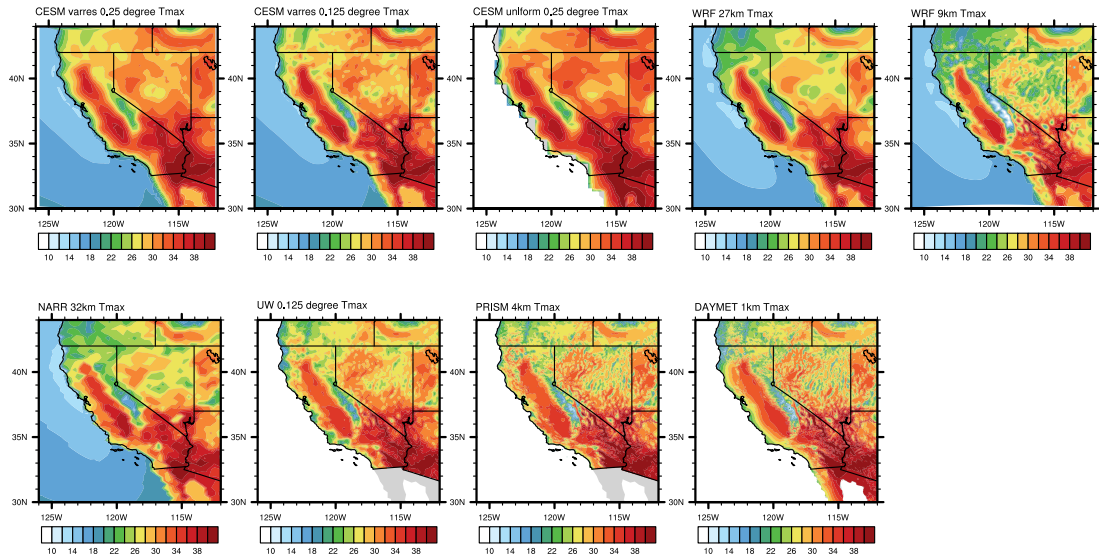


FIG. 9. Similar as Fig.4, but for summer Tmax

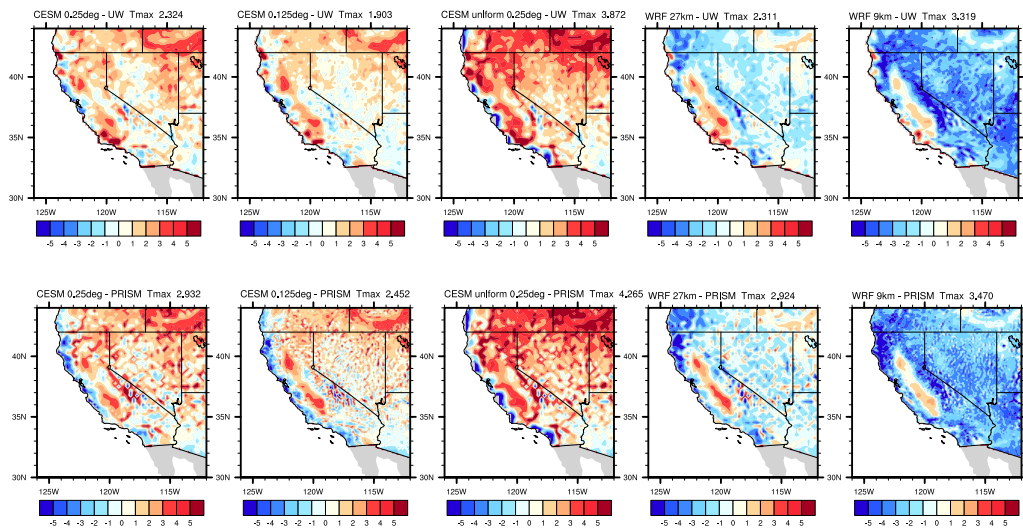


FIG. 10. Similar as Fig. 7 but for summer Tmax (the number is RMSE value)

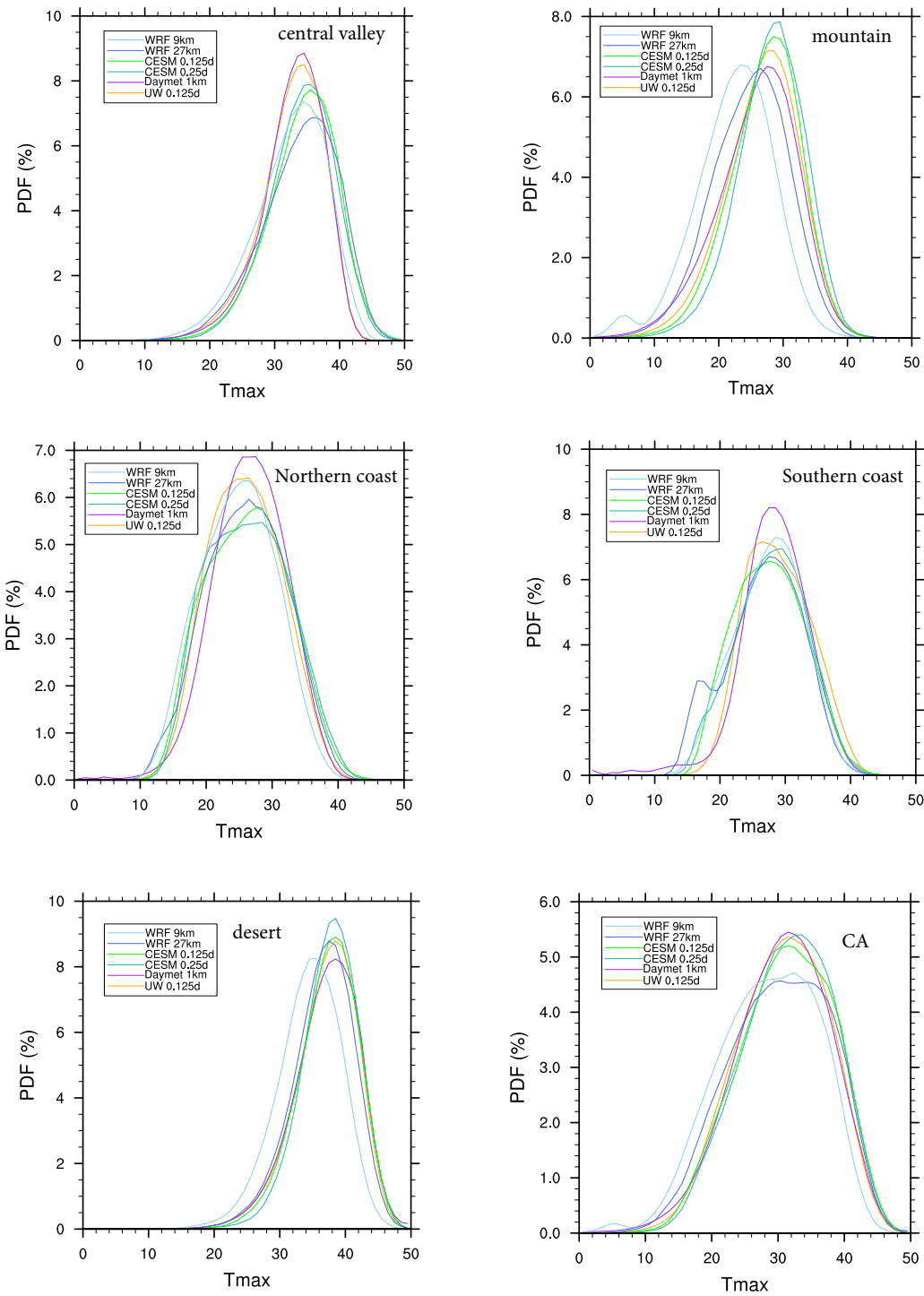


FIG. 11. Frequency distribution of summer Tmax constructed from 26 years daily data (unit: $^{\circ}\text{C}$)

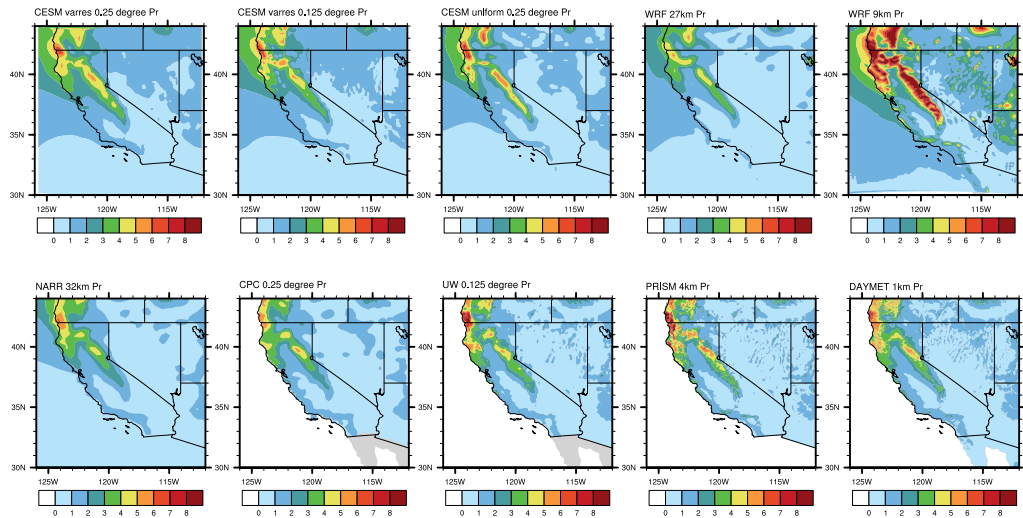


FIG. 12. Annual average daily precipitation (Pr) from models and reference datasets (unit: mm/d)

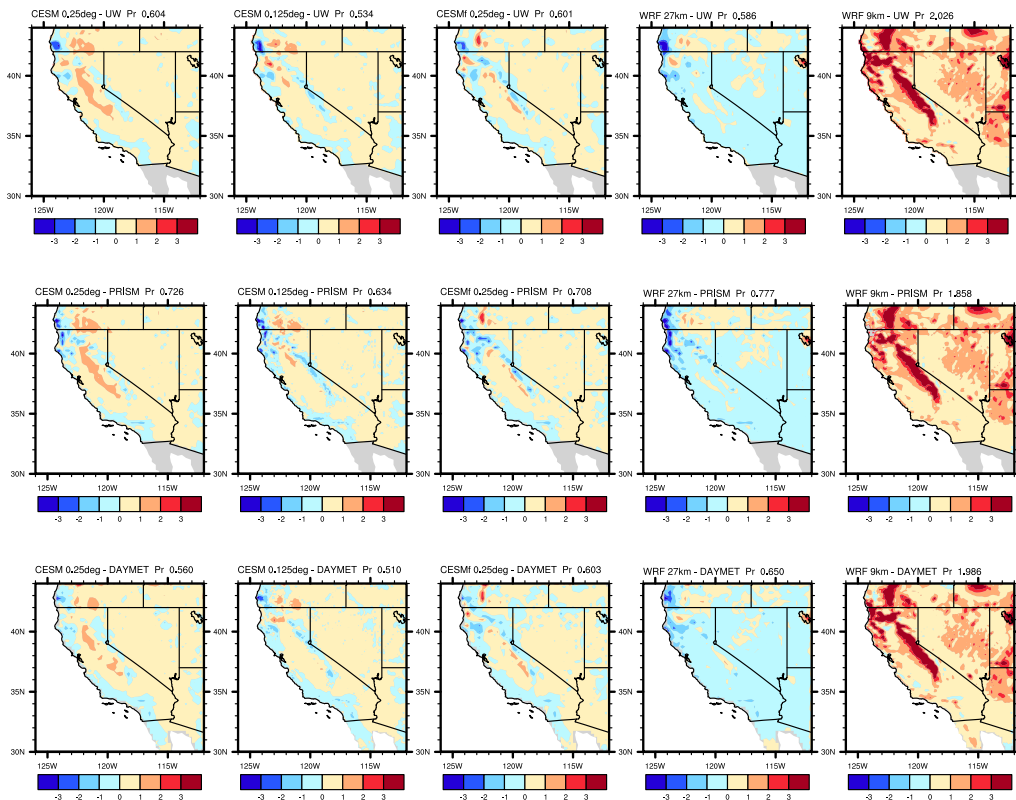


FIG. 13. Difference between simulations and reference data for Pr

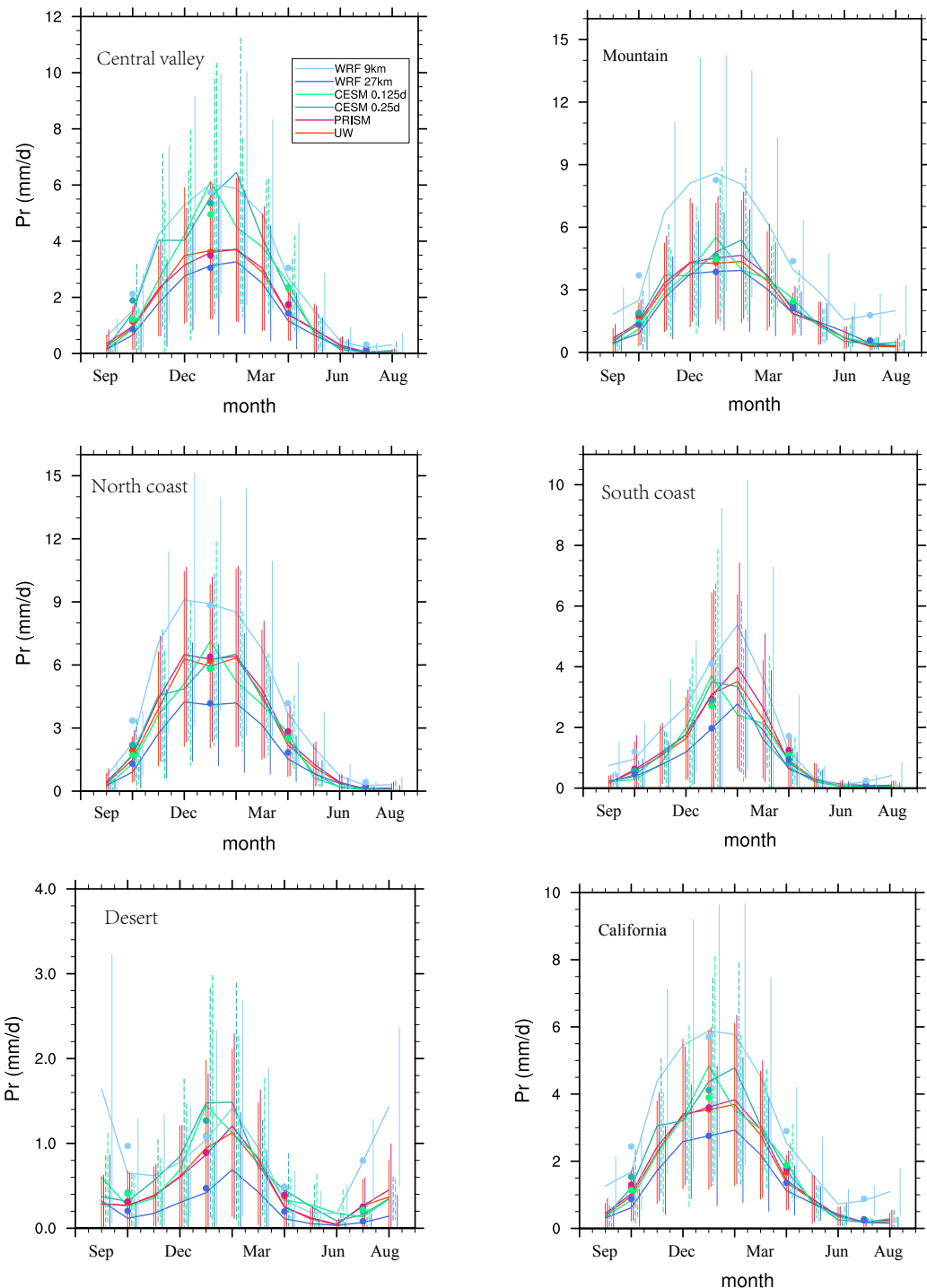


FIG. 14. Similar as Figure 8, but for monthly-average Pr

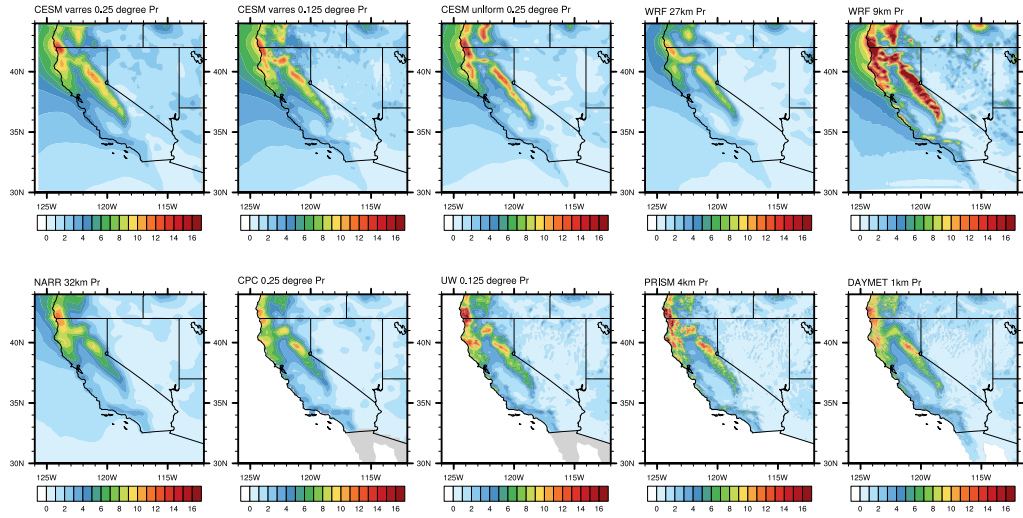


FIG. 15. Similar as Figure 12, but for winter Pr

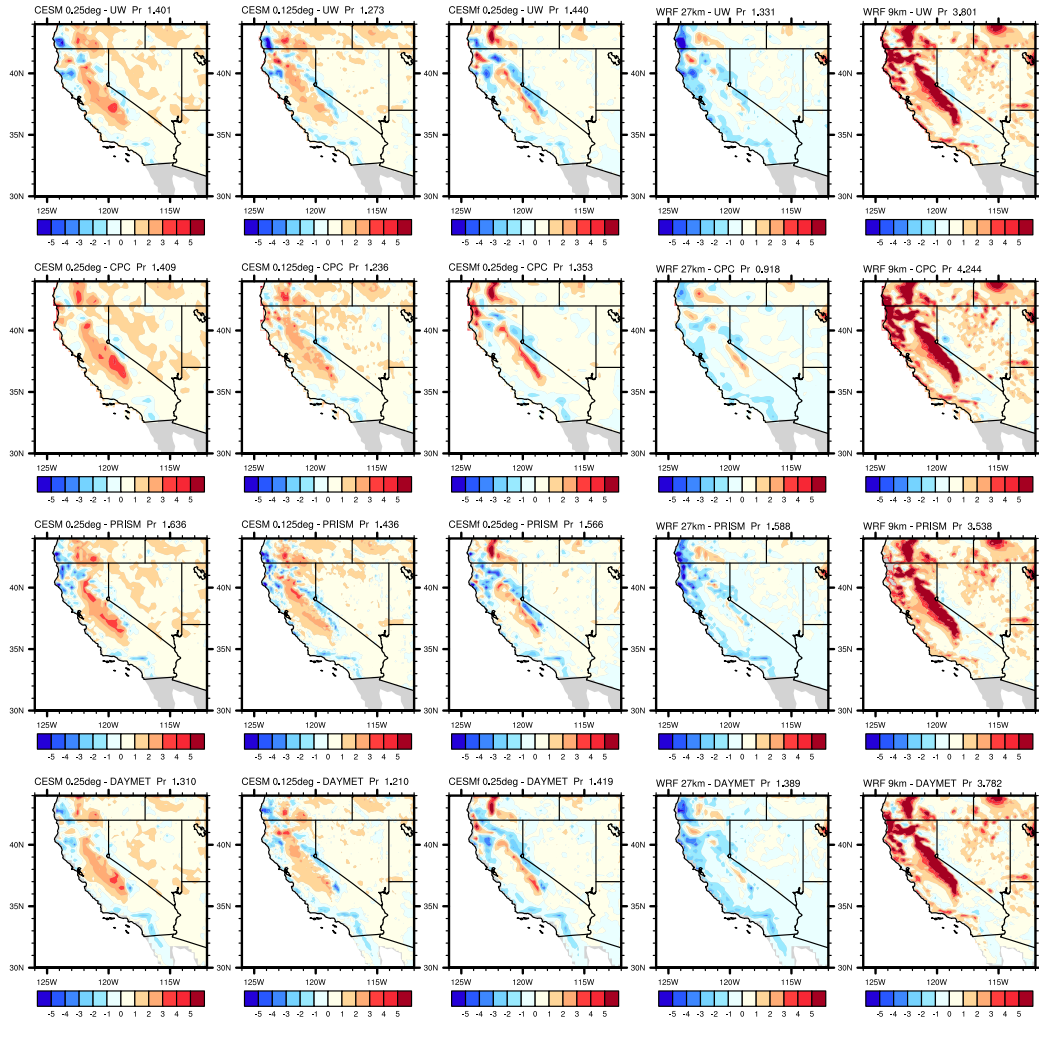
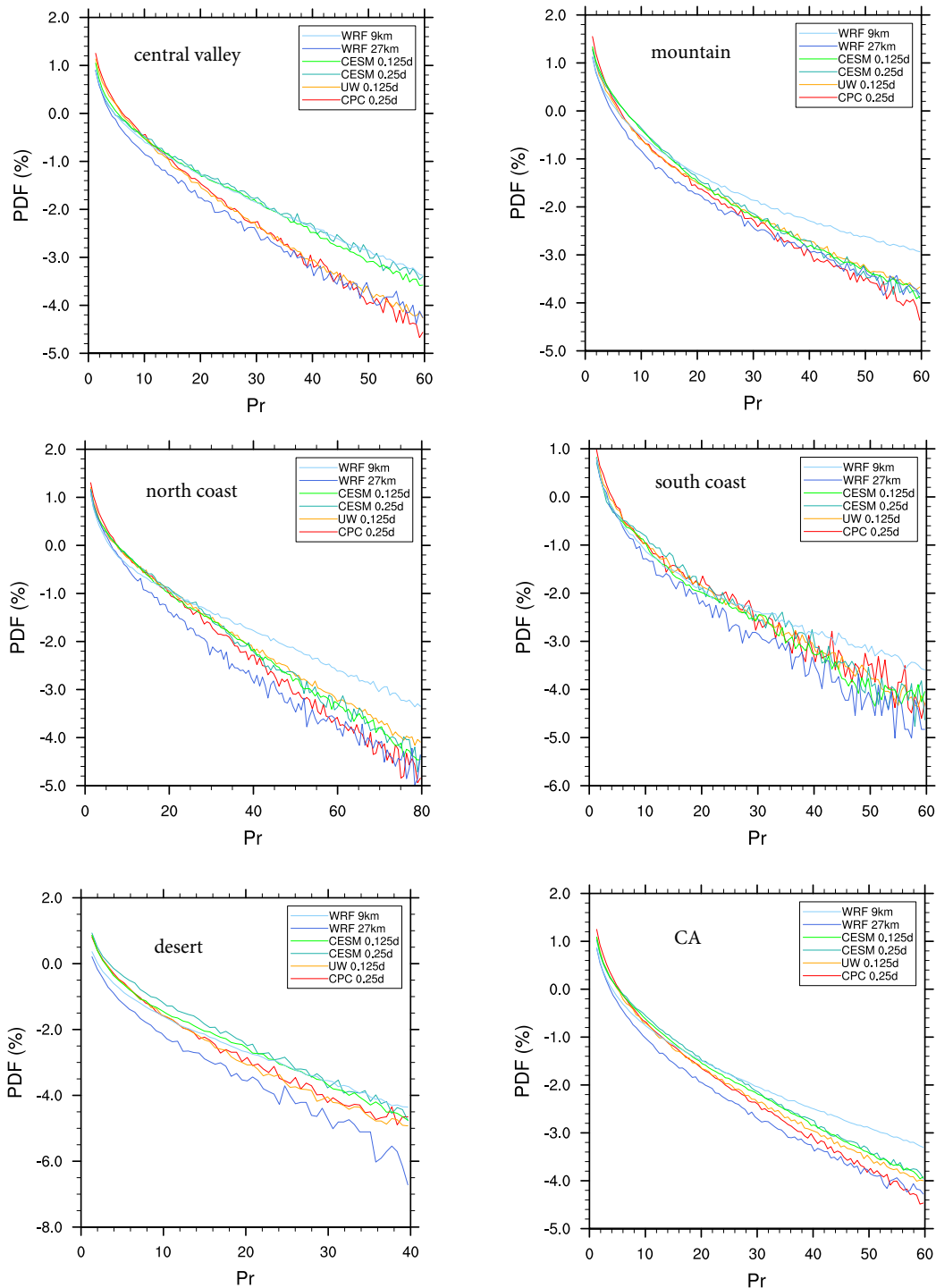


FIG. 16. Similar as Figure 13, but for winter Pr



396 FIG. 17. Frequency distribution of winter Pr constructed from 26 years daily data (unit: mm/d) (note: vertical
397 scale is logarithmic)

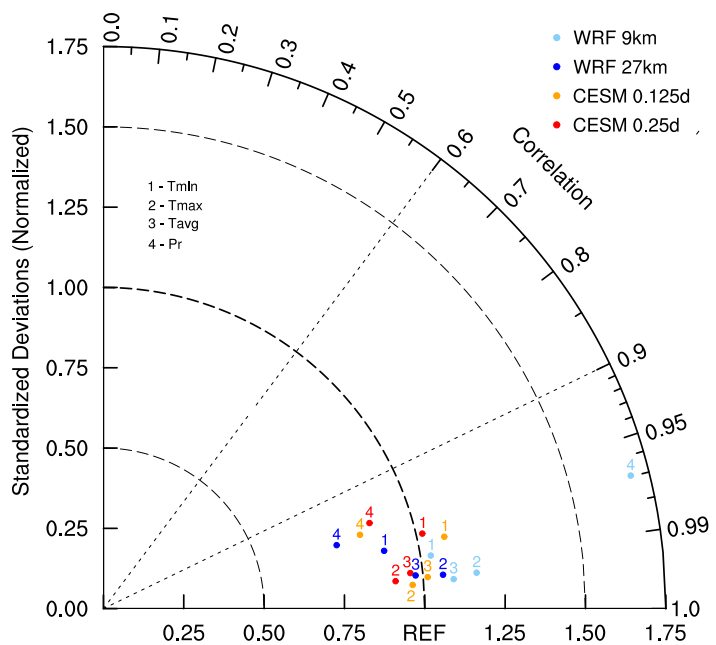


FIG. 18. Taylor diagram of annual climatology for the region of CA, using PRISM dataset as reference